

Article

Welding Properties of Dissimilar Al-Cu Thin Plate by a Single-Mode Fiber Laser

Soon-Jae Lee ¹, Kwang-Deok Choi ¹, Su-Jin Lee ^{1,*}, Dong-Sik Shin ¹ and Jae-Pil Jung ²

¹ Busan Machinery Research Center, Korea Institute of Machinery and Materials, Busan 46744, Republic of Korea

² Department of Materials Science and Engineering, University of Seoul, Seoul 02504, Republic of Korea

* Correspondence: leesj@kimm.re.kr

Abstract: To improve the reliability and safety of the electrical components used in automobiles, Cu and Al have recently been employed as electrodes, wherein lasers were used for rapid welding. However, in Al-Cu dissimilar metal welding, intermetallic compounds (IMCs) reduce the weld strength. In addition, the laser absorption rates of Al and Cu are low, and the reflectance is high, thereby impeding the welding process. To increase the absorption rate, a laser with a high beam quality must be used. Thus, a high-density, high-quality 5 kW single-mode laser was employed. Thin Al and Cu (0.2 mm thick) plates were processed and welded at welding speed 200–1000 mm/s, changing the laser-irradiated upper metal to Cu or Al. Post analysis, it was found that with a high heat input, pores were generated inside the Al, and when the upper metal was Cu, pores were mainly generated between the Al molten layer and the Cu mixed layer. As a result of tensile shear strength measurement, most of the aluminum area fractured at 118–151 N, and when fractured in copper, the strength was highest at 154 N. At a high welding speed, fracture was mainly observed at the joints along the IMCs or in the Cu mixed layer.

Keywords: laser welding; dissimilar welding; single-mode laser; aluminum; copper



Citation: Lee, S.-J.; Choi, K.-D.; Lee, S.-J.; Shin, D.-S.; Jung, J.-P. Welding Properties of Dissimilar Al-Cu Thin Plate by a Single-Mode Fiber Laser. *Metals* **2022**, *12*, 1957. <https://doi.org/10.3390/met12111957>

Academic Editor: Xiangdong Gao

Received: 25 October 2022

Accepted: 14 November 2022

Published: 15 November 2022

Publisher's Note: MDPI stays neutral with regard to jurisdictional claims in published maps and institutional affiliations.



Copyright: © 2022 by the authors. Licensee MDPI, Basel, Switzerland. This article is an open access article distributed under the terms and conditions of the Creative Commons Attribution (CC BY) license (<https://creativecommons.org/licenses/by/4.0/>).

1. Introduction

Recently, the electric vehicle market has grown in accordance with the European green car policies [1–3]. Although the use of electronic components inside vehicles with existing internal combustion engines has been steadily increasing, their usage is rapidly increasing with the arrival of electric vehicles [2–4]. Existing vehicles also employ batteries for various electronic components and internal devices. However, in the case of electric vehicles that use electricity as a power source, battery life and reliability are of particular importance [4,5]. Commonly, the electrodes of these batteries consist of Al, which is lightweight and easy to process, and Cu, which has high electrical conductivity; these two metals are joined together using a laser [2,4–7].

The main process parameters during laser welding include the power, speed, beam type, beam size, focusing distance, and focusing angle. The absorption/reflectance of the base material mainly depends on the wavelength of the laser beam. In this context, the wavelength of a typical industrial laser is approximately 1 μm, and the absorption rates of Al and Cu in this wavelength range are <5%. Particularly, in the case of Cu, the absorption rate is only ~2.5% [2,3]. In addition, even when the laser irradiation is absorbed by Al or Cu, high-speed and high-power welding are necessary because of the rapid cooling of the specimen, owing to its high thermal conductivity. In batteries, thin plates of Al and Cu are commonly used to reduce the battery weight and increase integration through lamination [5]. Thus, when welding Al and Cu thin plates, it is necessary to determine the optimum welding conditions because of the possibility of deformation caused by the welding heat, which can ultimately result in defects [2,6].

Fundamentally, welding dissimilar materials is more difficult than welding materials from the same material group. This can be attributed to the fact that the properties of each material and the reaction patterns before and after welding are different [2–4,6–10]. For example, intermetallic compounds (IMCs) are generated when dissimilar metals are joined, and these represent major defects during welding. However, because the generation of IMCs is inevitable in the welding of dissimilar materials, it is necessary to develop dissimilar welding conditions that minimize their formation. Since various IMCs can form depending on the materials employed, suitable welding conditions may be required [8,10–13].

IMCs are generally more brittle than metals, and they lack ductility and malleability. When IMCs are continuously generated to form a layer, cracks tend to proceed along the boundary, thereby resulting in the deterioration of the material mechanical properties [7–9]. To increase the weld strength, it is therefore necessary to control IMC formation; research is ongoing in this area. Since IMC formation varies with the amount and temperature of the molten metal, phase diagrams can be used to infer which IMCs are formed at specific temperatures and compositions [4]. However, owing to the difficulties involved in determining the temperature and metal composition at a specific point during instantaneous welding, IMCs can be traced backward by analyzing the compounds generated after welding. In addition, the temperature during welding and the composition of the molten metal can generally be controlled by controlling the amount of heat input [6,14–17]. Since the amount of heat input at the junction affects the viscosity of the molten metal, it also affects its composition [12,18].

When Al and Cu are used as battery electrodes, welding between these dissimilar metals is inevitable, and an IMC is produced. Previous research into IMC generation in the Cu–Al system has suggested that the Cu–Al IMC tends to be brittle, and several studies have been conducted to prevent this [2,4,7]. In addition, though the generation of an IMC is regarded as unavoidable, it may be possible to reduce the decrease in the mechanical strength by ensuring discontinuous generation of the IMC.

Laser welding is suitable for welding dissimilar materials with different melting points because it instantaneously joins the metals at high temperatures. Using a laser, the metals can be instantaneously heated to locally exceed the melting points of both materials, and a constant molten pool can be created [10,18–20]. If thin plates are joined for the preparation of dissimilar welding using lasers, the process conditions related to both the thin plates and the desired dissimilar welding must be considered. However, since the instantaneous high-temperature heat input of the laser can damage the thin plates, the amount of heat input should be carefully controlled. In addition, owing to the keyhole and repulsive pressure generated by the laser, a thin plate with a small molten pool can lead to joint failure [21]. Thus, to compensate for such welding difficulties, Cu–Al thin-plate welding is performed using a single-mode laser with a good beam quality.

There have already been many studies on the dissimilar welding of Al–Cu. However, in most studies, the laser was irradiated to Al rather than Cu to weld. This is because it is difficult to reach sufficient heat input due to the high reflectivity of Cu. In terms of thermal damage, irradiating a laser to Cu rather than irradiating a laser to Al may be advantageous in terms of damage to the base material. Research on Cu–Al dissimilar welding by irradiating a laser on the Cu side is also being conducted in various ways. When performing dissimilar welding by irradiating Cu with laser, coating Ni on the copper surface [22], controlling laser pulses [23], using wobble pattern [24], or brazing using filler metal [25,26] is used. In this study, a high-quality, high-density single laser was used, and the laser was irradiated to Cu with a thin plate capable of welding with at least the amount of heat input required to perform dissimilar welding. Weldability was studied when irradiating a laser to Cu and irradiating Al with a similar heat input without any treatment on Cu.

2. Materials and Methods

2.1. Materials

Al and Cu with purities of 99.99% were used as the base metals for the electrode. As shown in Figure 1b, the welding specimens measured $200 \mu\text{m} \times 50 \text{ mm} \times 70 \text{ mm}$, while the specimens used for the tensile shear strength tests were manufactured to have dimensions of $200 \mu\text{m} \times 20 \text{ mm} \times 50 \text{ mm}$. Table 1 shows the physical and mechanical properties of the base metals.

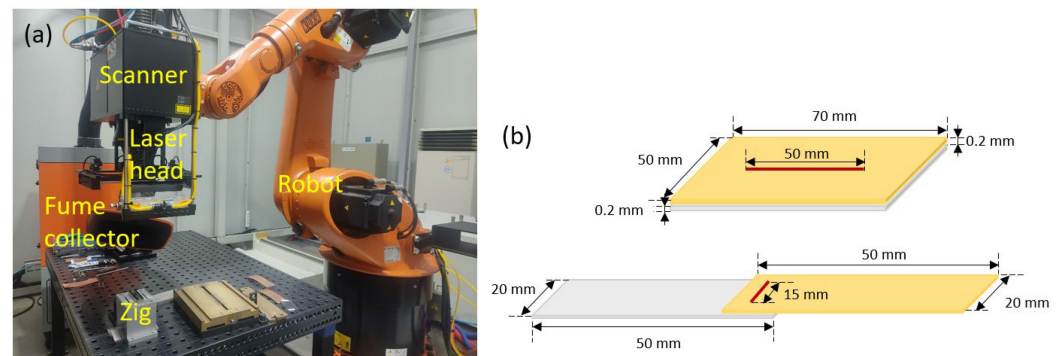


Figure 1. (a) Experimental setup for laser welding. (b) Dimensions of the welding specimen for the cross-section and tensile shear strength tests.

Table 1. Physical and mechanical properties of base metals.

Property	Al	Cu
Melting Point ($^{\circ}\text{C}$)	660	1085
Density (g/cm^3)	2.7	8.89
Thermal Conductivity (W/mK)	234	388
Resistance ($\Omega \text{ mm}^2/\text{m}$) $\times 10^2$	2.66	1.68
Tensile Strength (N/mm^2)	91.5	220.5
Hardness (HV)	57.98	106.90
Elongation (%)	30.10	36.67

The surface of each specimen was cleaned with acetone prior to welding. After welding, the joint was cut and mounted with epoxy resin for cross-sectional analysis. The mounted specimen was ground with 500, 1200, and 2400 sandpaper and then polished with $3 \mu\text{m}$ alumina powder. Each specimen was examined using a microscope to measure the size and width of the welding joints, and micro-analysis was performed using field emission scanning electron microscopy (FESEM, SU5000, HITACHI, Tokyo, Japan) and energy-dispersive X-ray spectroscopy (EDS, SU5000, HITACHI, Tokyo, Japan). After measuring the tensile shear strength, the fractured specimen was processed and analyzed in a manner similar to that described above to confirm the fracture site.

2.2. Laser Welding

The laser used for welding was a single-mode fiber laser (YLS-5000-SM, IPG, Oxford, MA, USA) that can output power of up to 5 kW. The wavelength of the laser beam was 1070 nm, and the spot size was $30 \mu\text{m}$. Welding was performed at the desired focal length, and the experiment was conducted while changing the laser power and speed. The scanner (KScan-300, KLab, Gyeonggi-do, Republic of Korea) was equipped with a robotic arm (KUKA Roboter GmbH, Augsburg, Germany) and was operated using the associated operating software (HK welding system, Intech Automation, Gyeonggi-do, Republic of Korea). No shielding gas was used, but air was blown into the scanner to protect the laser head. The laser welding system is shown in Figure 1a. The experiments were carried out by changing the laser-irradiated material to Cu or Al or by decreasing the welding speed by 200 mm/s from the speed of 1000 mm/s, where welding was not

possible. All experiments were performed at a laser power of 2 kW. Table 2 summarizes the experimental conditions employed during this study.

Table 2. Laser welding parameters.

Parameter	Upper Material	Welding Speed (mm/s)
1	Al	200
2	Al	400
3	Al	600
4	Al	800
5	Al	1000
6	Cu	200
7	Cu	400
8	Cu	600
9	Cu	800
10	Cu	1000

3. Results

3.1. Cross-Sectional Analysis

3.1.1. Macro Analysis

The cross-sectional images of the welding beads obtained under the various investigated conditions are shown in Figure 2. The region of molten Al was defined by EDS as the portion containing a trace amount of Cu inside the Al. The length of the molten area was measured as the length of the part where the Al was exposed to the outside. The length of the molten Al region is the average of three random point measurements of the joint. As shown, when Al is used as the upper material, and a welding speed of 200 mm/s is employed, the length of the melted Al area reaches 656 μm . Upon increasing the welding speed from 400 to 800 mm/s, a melt length ~ 450 μm is obtained, and this reduces further to 341 μm at a welding speed of 1000 mm/s. When Cu is used as the upper material, the length of the Al melting area is 487 μm at a welding speed of 200 mm/s, and this area gradually decreases to 146 μm at 800 mm/s. In addition, at a welding speed of 1000 mm/s, the weld is only partially joined.

Using an optical microscope, it is possible to distinguish between Al and Cu, which solidify at the junction after melting. In the molten Cu area, Cu and the Cu-Al IMC are present as a mixture. In both conditions (i.e., with either Al or Cu on top), a junction is formed that consists of molten Cu (i.e., Cu + Al-Cu IMC) penetrating the Al layer. As shown in Figure 2a, the IMC content increases throughout the mixed area, although it is distributed in a relatively nonuniform manner. However, when a high welding speed is employed, Al infiltrated into the Cu layer (Figure 2e).

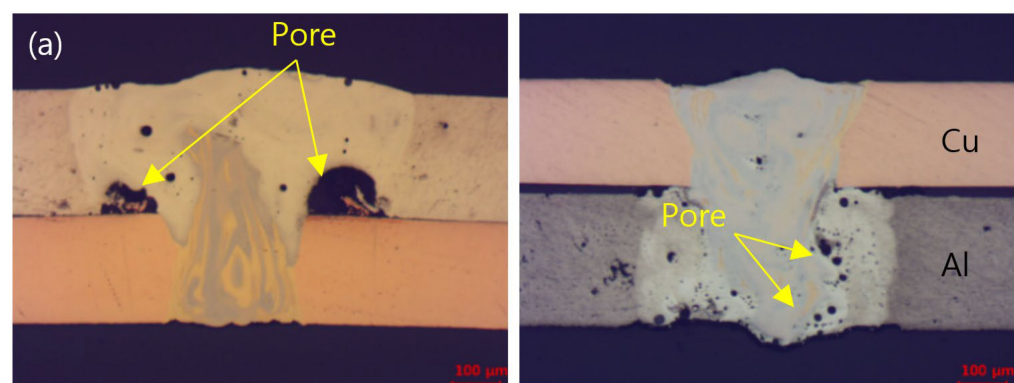


Figure 2. Cont.

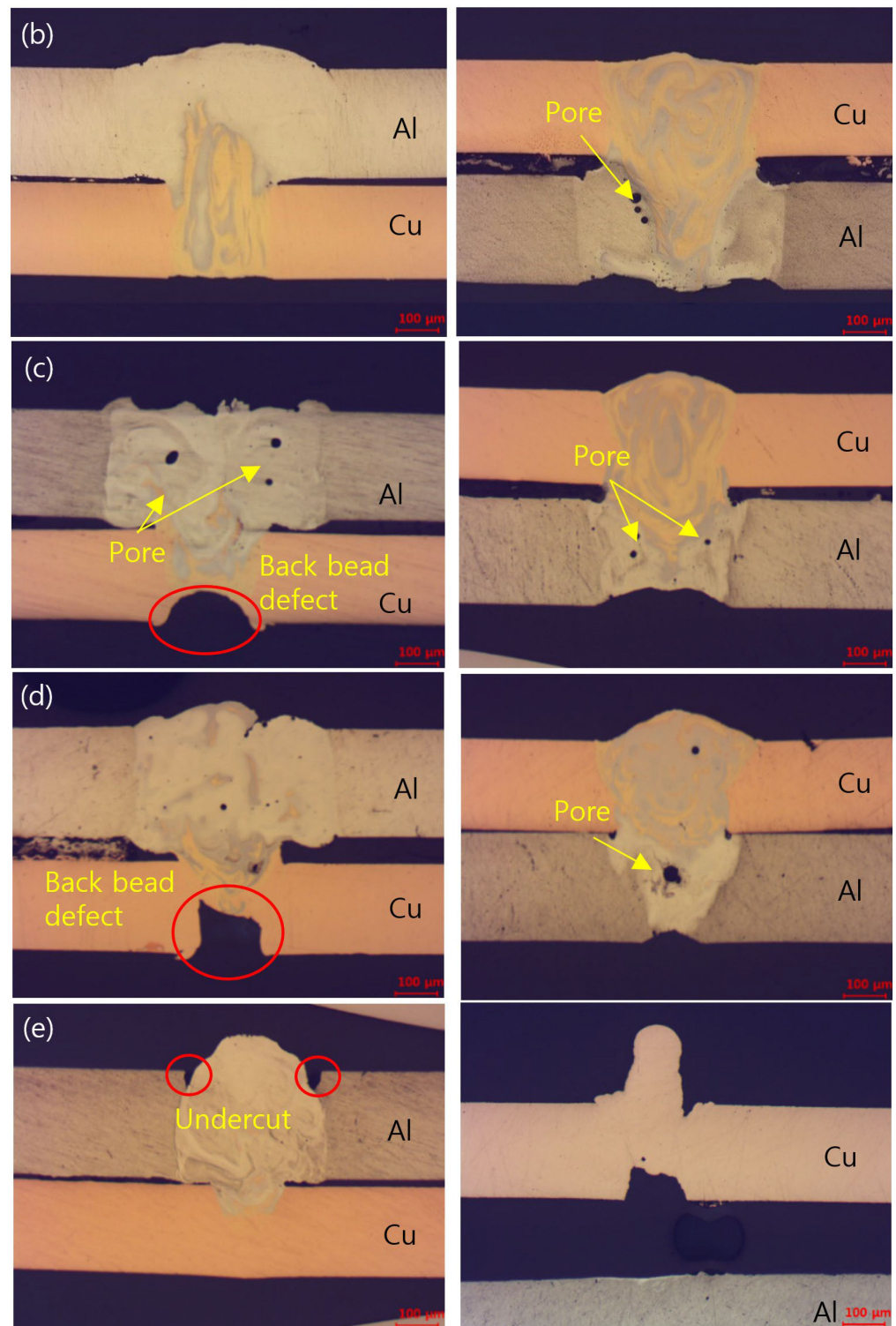


Figure 2. The cross-sectional images recorded under different welding conditions. The left-hand images show Al as the upper material, while that of the right-hand show Cu as the upper material. The welding speeds employed in each pair of images were as follows: (a) 200 mm/s, (b) 400 mm/s, (c) 600 mm/s, (d) 800 mm/s, and (e) 1000 mm/s.

In addition, from Figure 2a, it is deduced that pores with diameters of 100–150 μm are generated in the Al molten zone. More specifically, depending on the melting point and cooling rate during the welding process, pores form between the solid Cu area and the molten Al. When Al is used as the upper material, several pores with a diameter of $\leq 10 \mu\text{m}$

are generated in the molten Al area but are sparse in the molten Cu area. In contrast, when Cu is used as the upper material, pores mainly form between the mixed zone of Cu (i.e., the molten Cu area) and the molten Al area and are found along the melt boundary. As shown in Figure 2d, pores are also observed in the center of the molten Al area.

Furthermore, the presence of back-bead defects is confirmed in the Cu layer when Al is used as the upper material (Figure 2b,c). In the presence of these defects, the upper part of the bead becomes unstable. Moreover, at a welding speed of 1000 mm/s, an undercut is observed in the partially welded joint, as shown in Figure 2e.

3.1.2. Composition Analysis

Figure 3 shows the results of the EDS mapping carried out post specimen preparation for the joint cross-sections after welding at a speed of 400 mm/s. More specifically, Figure 3a shows that Cu is uniformly distributed inside the molten Al area. Conversely, in the Cu molten area, there is a nonuniform distribution of Al, which represents the IMC. As shown in Figure 3b, Cu was detected along the IMC layer generated in the molten Al area. Al was also detected in the IMC layer in the molten Cu area. However, the amount is smaller than that of Cu detected in the molten Al area. In addition, when Cu is used as the upper material, it is confirmed that the IMC layer is distributed as if it is sinking to the bottom of the joint.

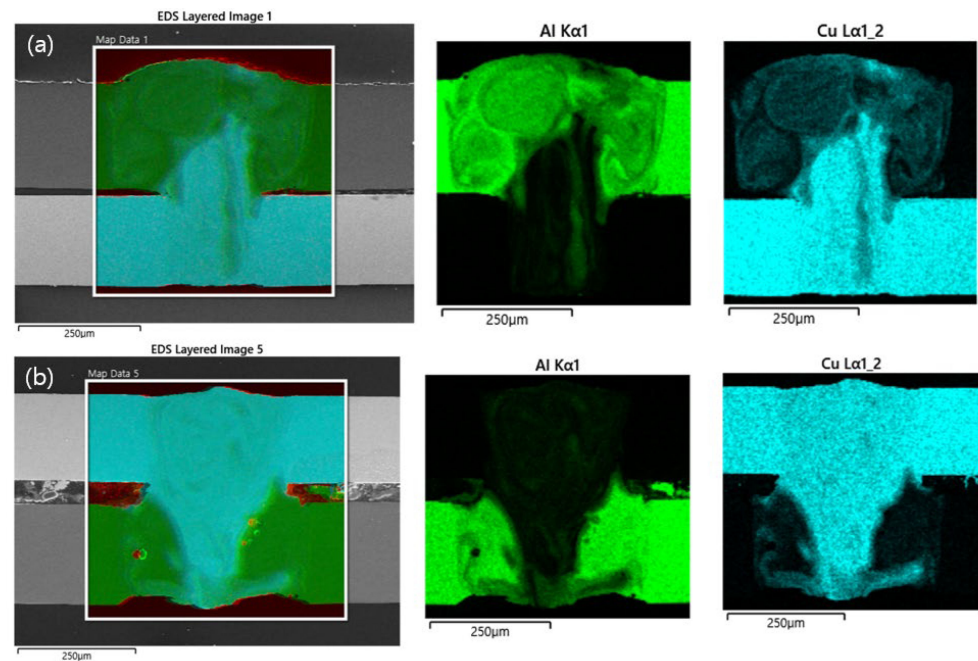


Figure 3. Energy-dispersive X-ray spectroscopy (EDS) mapping images for the joint cross-sections showing the distributions of Al and Cu after welding at a speed of 400 mm/s. (a) Using Al as the upper materials, and (b) using Cu as the upper material.

3.2. Strength

3.2.1. Tensile Shear Strength

Tensile shear strength evaluations were performed for the various specimens, and the results are listed in Table 3. The strength test is carried out by referring to ISO 14329:2003 suitable for thin plate. It should be noted here that partially welded specimens, namely those produced at a welding speed of 1000 mm/s, were not subjected to these measurements. As shown in the table, except for the welding speed of 200 mm/s, the strength is marginally higher when Cu is used as the upper material. In addition, all specimens are found to fracture in the Al base metal, except at a welding speed of 800 mm/s. Furthermore, when Al is used as the upper material with a welding speed of 800 mm/s, the joint fractures. Conversely, when Cu is used as the upper material under the same conditions, the base metal fractures.

Table 3. Results of the tensile shear strength tests.

No.	Parameter		Force (N)			Fracture Area
	Upside	Speed (mm/s)	Min	Max	Average	
1	Al	200	125.8	148.0	138.0	Al
2	Al	400	118.2	152.1	137.3	Al
3	Al	600	129.9	149.9	142.0	Al
4	Al	800	143.6	131.7	137.7	Joint
5	Al	1000	-	-	-	-
6	Cu	200	126.4	133.8	132.8	Al
7	Cu	400	144.4	144.2	151.8	Al
8	Cu	600	150.0	138.6	148.1	Al
9	Cu	800	153.8	142.8	154.4	Cu
10	Cu	1000	-	-	-	-

3.2.2. Fracture Morphology

The cross-sections of three fractured specimens after the tensile shear strength test are shown in Figure 4. More specifically, as shown in Figure 4b, joint fracture occurs because of the insufficient melting of Cu, which in turn is attributed to the low heat input. In contrast, for the specimen that fractures in the Al base metal (Figure 4a), no breakage is observed in the molten Al area, with all fractures instead forming outside this Al area. However, despite crack formation in the Al base metal, the cracks propagate along the IMC layer created inside the molten Cu zone. Furthermore, the specimen that fractures in the Cu base metal exhibits crack formation along the IMC layer that is inside the molten Cu zone. Finally, crack propagation occurs along the IMC layer, although necking is observed prior to ductile failure in the Al base metal.

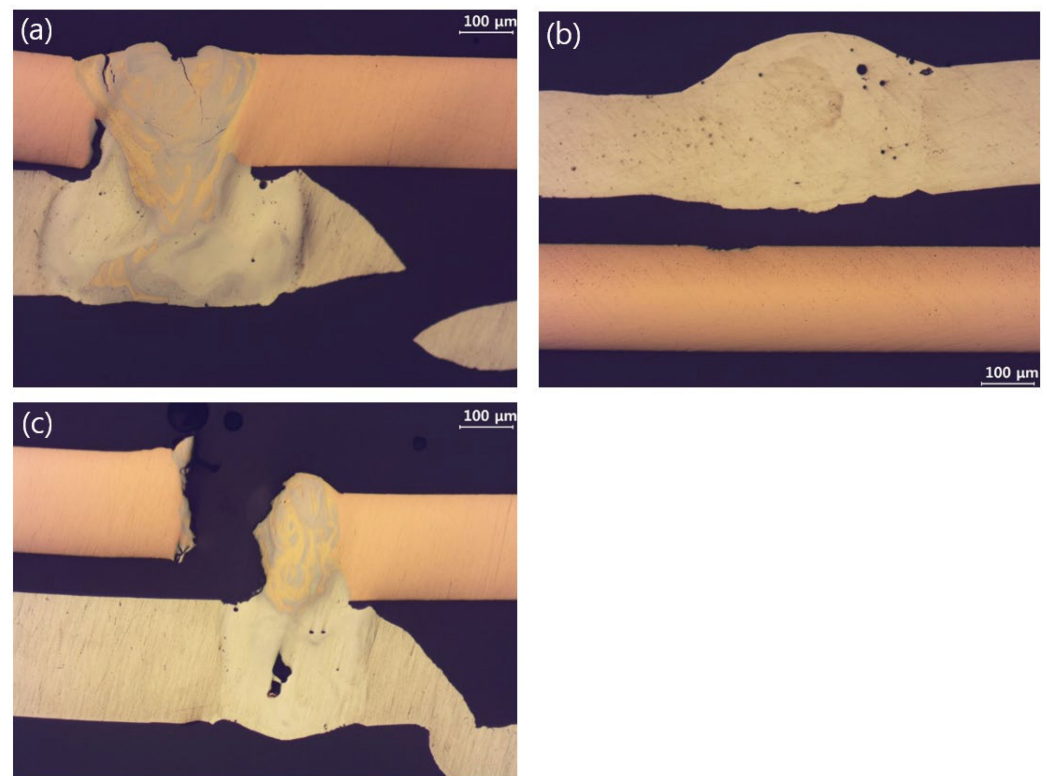


Figure 4. Cross-sectional images of fracture specimens, with fracture formation in (a) the Al base metal (Cu-Al, 2 kW, 200 mm/s), (b) the joint (Al-Cu, 2 kW, 800 mm/s), and (c) the Cu base metal (Cu-Al, 2 kW, 800 mm/s).

4. Discussion

4.1. Molten Pool

The laser power and welding speed employed during welding determine the amount of heat input into the metals [14–17]. In a general welding process, and particularly when the energy source is an arc, the amount of heat input can be expressed by Equation (1):

$$Q = k \frac{U \times I}{v} \quad (1)$$

where the heat input Q is proportional to the arc voltage (U) and the arc current (I) and is inversely proportional to the welding speed (v). Here, k is a constant related to the welding process.

During arc welding, the amount of heat input is represented by the arc energy received by the base metal. However, in the case of laser welding, if the energy used for welding is calculated using Equation (1), the amount of energy used for welding will be different [10–12]. This is because the reflection and absorption rates for the wavelengths differ depending on the base metal. Equation (1), therefore, cannot be used in laser welding because it does not contain any reference to the properties of the base metal. Particularly, in the case of dissimilar metal welding, the reflectance/absorption rate differs depending on the base metal. Therefore, even if the same laser is used for irradiation purposes, the energy received by the base materials can differ. In addition, because the laser is out with the focus range while melting the base metal, there is also an output difference between the laser irradiation received by the upper and lower metal layers.

In terms of laser welding, the laser power and the welding speed are important because they are related to the conditions responsible for keyhole formation. In this context, Nakayama et al. studied the principle of keyhole formation [20], while Fabbro et al. confirmed the effect of the welding speed on keyhole formation [27–29]. Figure 5 depicts keyhole formation with respect to the welding speed. The reflection of the laser range was adjusted according to the welding speed, thereby affecting the creation of keyholes. In this figure, the vertical axis represents the laser power, the horizontal axis represents the welding speed, and the keyhole shape is classified according to its aspect ratio.

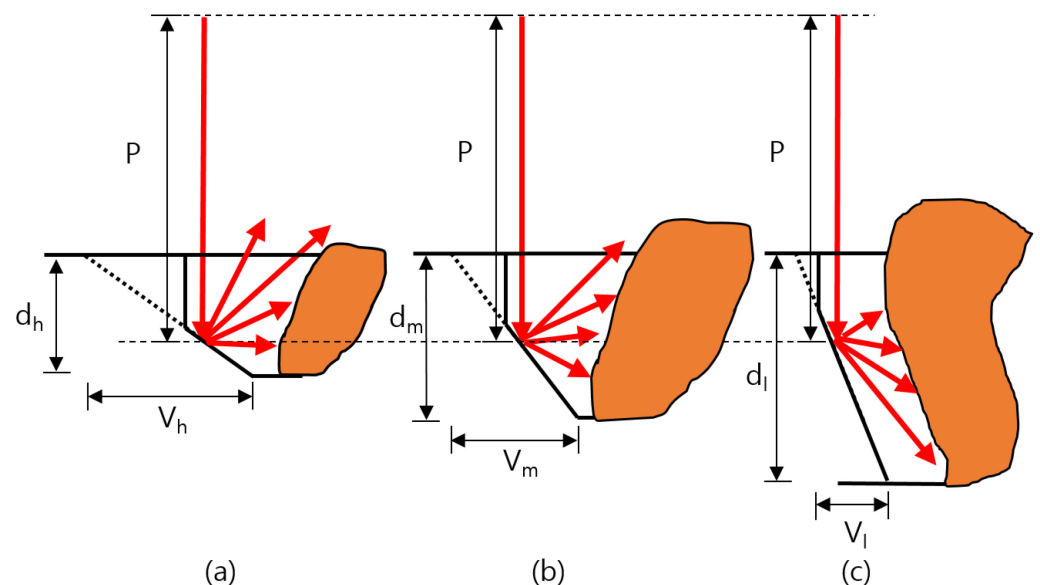


Figure 5. Keyhole formation at different welding speeds. The welding speed are represented by (a) V_h , (b) V_m , and (c) V_l , where $V_h > V_m > V_l$.

Previously, Katayama et al. studied the behavior of the molten pool and confirmed the formation of trapped pores [20]. In the case of Al-Cu dissimilar welding, the majority

of pores form inside the Al layer. This can be accounted for by considering that under cooling at high temperatures, Cu is the first metal species to exhibit cooling, and owing to its significant pore content, pores are generated within the Cu component inside the subsequently cooled Al layer. Therefore, when Al was used as the upper material, the Cu component existed intermittently inside the Al, and when Al was used as the bottom material, the pores rose and met the mixed Cu zone to exist along the interface. Furthermore, during dissimilar welding, the molten Al and solid Cu come into contact, as shown in Figure 2a. Owing to the different melting points of Al and Cu, in addition to their different laser absorption rates, their melting areas differ, and trapped pores are formed in the area where the Al and Cu base materials meet. This process appears to occur more significantly when the melting points between the base metals is particularly large.

4.2. IMC

Figure 6 shows the EDS mapping results that confirm the distribution of the IMC layer created inside the weld. In addition, Table 4 shows the results of the EDS point analysis, which confirm the formation of CuAl_2 . Thus, as shown in Figure 6b,c, the $\alpha(\text{Cu})$ phase, the CuAl_2 phase, and the $\text{Al} + \text{CuAl}_2$ can be seen. When welding is carried out using Al as the upper material, Cu is uniformly distributed throughout the area, with the exception of the area where the molten Cu has penetrated the Al melt. This detection of Cu in trace amounts throughout the specimen can be attributed to two key factors: (1) When Al is cooled, the produced IMC is partially dissolved in the molten Al; and (2) the fumes generated from the lower Cu layer during welding are dissolved inside the molten Al.

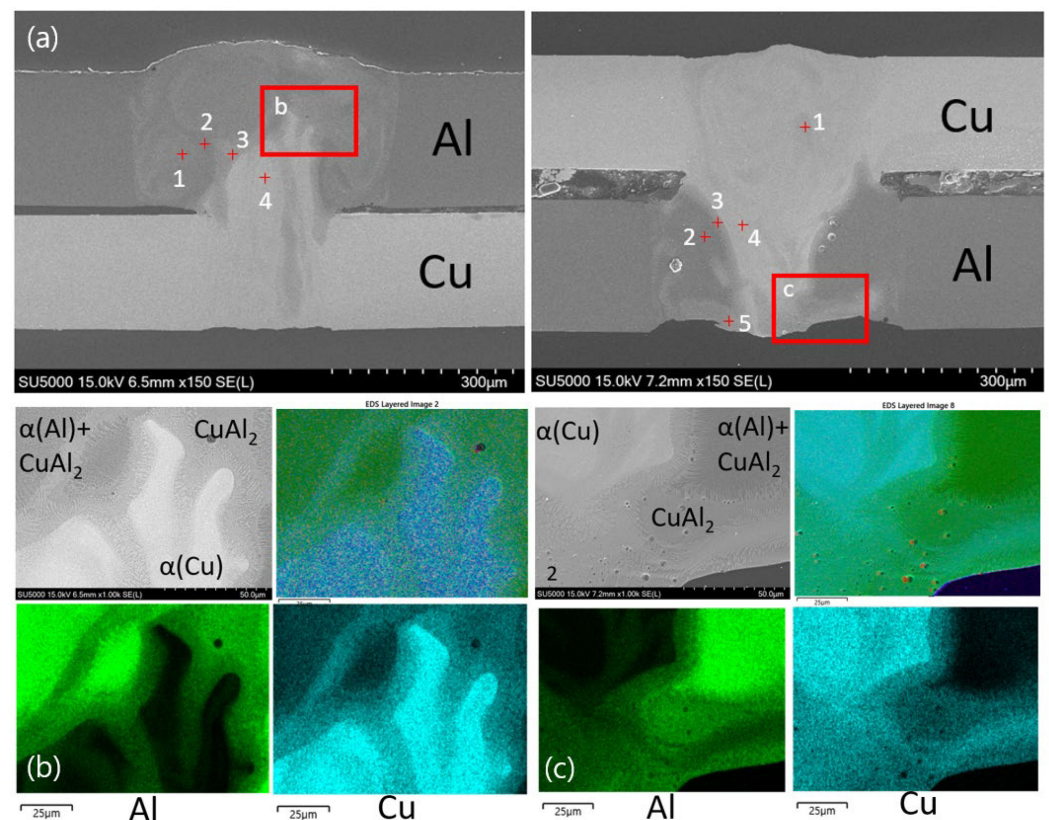


Figure 6. (a) Scanning electron microscopy images of the welded specimens. (b,c) EDS mapping images showing the distribution of Al and Cu to observe phase formation at a welding speed of 400 mm/s with: (b) Al as the upper layer, and (c) Cu as the upper layer.

Table 4. EDS point analysis and phase identification.

Atomic%	Al	Cu	C	O	Phase
1 (Al-Cu)	72.21	6.63	20.16	1.00	α -Al + CuAl ₂
2	73.08	5.76	20.16	1.00	α -Al + CuAl ₂
3	48.61	24.26	25.91	1.22	CuAl ₂
4	15.61	49.06	34.15	1.18	α -Cu + CuAl ₂
1 (Cu-Al)	20.83	46.82	32.35	-	α -Cu + CuAl ₂
2	75.73	3.01	18.91	2.35	α -Al + CuAl ₂
3	17.30	49.40	32.13	1.17	α -Cu + CuAl ₂
4	20.57	47.16	32.27	-	α -Cu + CuAl ₂
5	56.98	13.82	27.83	1.37	α -Al + CuAl ₂

As shown in Figure 6c, EDS analysis confirmed that the Cu mixed zone is spread along the lower Al layer. Since the Cu mixed phase is heavier than the molten Al, it spreads downwards. However, it should be noted that the actual behavior of the molten pool is affected by the pressure inside the keyhole that is generated during welding. Thus, since full penetration welding for a thin plate has no bottom, it can be assumed that recoil pressure is generated toward the hole at the bottom, and that this pressure pushes the molten pool downwards.

In dissimilar welding, IMC generation is an important factor in determining the ductile or brittle fracture properties of the specimen, in addition to its overall strength. We therefore wished to determine the influence of the welding conditions on the formation of propagation of ductile and brittle fractures [13,16]. To measure the specimen strength, the area of the bonding surface was divided by the obtained fracture strength, since it is known that the strength varies depending on the components present within the bonded area. However, during laser welding, the joint area varies depending on the experimental conditions, including the laser power and welding speed [27–29]. As shown in Figure 4b, joint fracture does not take place because of the joint composition, but rather because the joint area is insufficient. The overall strength result for this specimen indicates that the fracture forms at ~140 N due to the thickness of the Al base material, and the strength differs according to the degree of softening imparted by the laser [19]. In contrast, it can be seen in Figure 4c that fracture formation also took place in the Cu base metal. It should be noted that although both Al and Cu fractures are considered to be base metal fractures, the Cu base metal fracture is similar to the joint fracture because the fracture occurs at the Cu fusion zone along the IMC layer.

The strength of dissimilar metal bonding is generally determined by the degree of IMC formation. However, in the case of thin plates, the thickness of the base material does not significantly differ from the length of the joint area (i.e., ~200 μ m), and as a result, the base metal easily fractures [7–10,19]. In particular, Al fracture on Al occurs because of the low strength, good ductility, and malleability of this metal. However, as shown in Figure 4a,c, cracks also form in the IMC layer, even when Al fracture occurs. In addition, the specimen that undergoes fracture in the Cu layer was found to fracture along the IMC, as described above. Overall, fracture along the IMC can be accounted for by considering two key points. Firstly, the thermal effect on Al is less than that of the other metal, and as a result, softening is minimized and the strength is increased, thereby leading to fracture in the IMC. Alternatively, it can be inferred that the IMC is continuously generated and fractures when the amount of heat input is insufficient or the cooling rate is fast, since fracture of this component is generally observed at a welding speed of ≥ 800 mm/s. However, when fracture occurs at the Cu side of the joint, the strength slightly increases compared to when Al fractures are present. As a result, the degree of Al softening by the laser is considered small, and the strength of Al relatively increases to result in fracture of the IMC layer [13,15].

During laser welding, the bonding area is determined by the laser beam size, and many attempts have been made to increase the bonding area by increasing the beam. This

could be achieved by using a wobble that repeatedly heats the junction, or through the development of a corona beam. Alternatively, defocus could be used to reduce the output and increase the beam size or expand the area through conduction welding. However, in the case of the thin Al plate, the strength of the Al base metal softened by the laser is reduced despite the narrow bonding area and the generated IMC. Thus, even in the case where Al is employed by industry to obtain increased strengths, the deformation of Al occurs, rather than destruction through the IMC. Thus, if an alternative impact or bending strength measurement is chosen instead of the tensile shear strength, the IMC generation could prove to be fatal to the material. It is therefore necessary to study the properties of laser-welded Al alloys that exhibit higher strengths compared to that of pure Al.

5. Conclusions

In this study, Al-Cu dissimilar welding were performed using a high-quality 5 kW single-mode laser. The characteristics were analyzed according to the laser-irradiated base material and welding speed.

- (1) When bonding was performed while increasing the speed at the same output of 2 kW, the amount of heat input decreased, and when the speed reached 1000 mm/s, the bonding was not performed with a certain base metal on the top.
- (2) Pores were observed according to the experimental conditions, and when the amount of heat input was large, they were generated inside the Al or adjacent to the Cu mixed zone, and the pores were generated between the unmelted Cu in the Al molten layer. When the laser was irradiated to Al at a speed of 400 mm/s, a cross section without pores was obtained.
- (3) As a result of EDS mapping analysis, it was confirmed that Cu was distributed in a very small amount when Al was on the top, which is thought to be due to fume. When Cu was on the top and full penetration was achieved to the Al on the bottom, it was confirmed that Cu existed along the bottom surface, and the recoil pressure inside the keyhole exerted downward influence.
- (4) As a result of EDS analysis, it was confirmed that CuAl_2 was spread inside the Al and Cu phases or existed between the two phases in the form of a layer inside the weld.
- (5) As a result of the tensile shear strength test, fracture occurred on the Cu side at the speed of 800 mm/s when Al was on the top of the joint, and when Cu was on the top. Specimens fractured in the Al base metal were fractured in the softened area inside the heat-affected zone, not the molten area, and fractures occurred in the area where Cu was melted and IMC was generated inside.

Author Contributions: Conceptualization and methodology, S.-J.L. (Soon-Jae Lee) and S.-J.L. (Su-Jin Lee); validation, S.-J.L. (Soon-Jae Lee) and J.-P.J.; investigation, S.-J.L. (Su-Jin Lee) and K.-D.C.; writing—original draft preparation, S.-J.L. (Soon-Jae Lee) writing—review and editing, S.-J.L. (Su-Jin Lee) and D.-S.S. All authors have read and agreed to the published version of the manuscript.

Funding: This research was funded by “Welding technology development using coaxial dual beam and visible laser” (code:20012887) of KEIT (Korea Evaluation Institute of Industrial Technology).

Institutional Review Board Statement: Not applicable.

Informed Consent Statement: Not applicable.

Data Availability Statement: Not applicable.

Acknowledgments: This work was supported by “Technology platform for advanced laser beam process of metallic fuel cell plates” (code: P0012884, Eurostars2) of KIAT (Korea Institute for Advancement of Technology) and “Welding technology development using coaxial dual beam and visible laser” (code:20012887) of KEIT (Korea Evaluation Institute of Industrial Technology).

Conflicts of Interest: The authors declare no conflict of interest.

References

1. Lee, S.-J.; Choi, K.-D.; Park, B.-H.; Kim, J.-D.; Suh, J. Weldability of aluminum alloys laser welding for with high-power disk laser. *J. Korean Soc. Mar. Eng.* **2017**, *41*, 638–645.
2. Kang, M.J.; Choi, W.S.; Kang, S.H. Ultrasonic and Laser Welding Technologies on Al/Cu Dissimilar Materials for the Lithium-Ion Battery Cell or Module Manufacturing. *J. Weld. Join.* **2019**, *37*, 52–59. [[CrossRef](#)]
3. Lee, S.-J.; Kim, J.-D.; Katayama, S. A Study on the Characteristic of Weld Joint and Tensile Fracture of SUS304 and Cu High-Speed Dissimilar Lap Welds by Single Mode Fiber Laser. *J. Weld. Join.* **2014**, *32*, 56–63. [[CrossRef](#)]
4. Dimatteo, V.; Ascari, A.; Fortunato, A. Continuous laser welding with spatial beam oscillation of dissimilar thin sheet materials (Al-Cu and Cu-Al): Process optimization and characterization. *J. Manuf. Process.* **2019**, *44*, 158–165. [[CrossRef](#)]
5. Knaak, C.; von Eßen, J.; Kröger, M.; Schulze, F.; Abels, P.; Gillner, A. A Spatio-Temporal Ensemble Deep Learning Architecture for Real-Time Defect Detection during Laser Welding on Low Power Embedded Computing Boards. *Sensors* **2021**, *21*, 4205. [[CrossRef](#)]
6. Firouzdar, V.; Kou, S. Al-to-Cu Friction Stir Lap Welding. *Metall. Mater. Trans. A* **2012**, *43*, 303–315. [[CrossRef](#)]
7. Lee, S.J.; Nakamura, H.; Kawahito, Y.; Katayama, S. Effect of welding speed on microstructural and mechanical properties of laser lap weld joints in dissimilar Al and Cu sheets. *Sci. Tech. Weld. Join.* **2014**, *19*, 111–118. [[CrossRef](#)]
8. Lee, S.-J.; Takahashi, M.; Kawahito, Y.; Katayama, S. Microstructural Evolution and Characteristics of Weld Fusion Zone in High Speed Dissimilar Welding of Ti and Al. *Int. J. Precis. Eng. Manuf.* **2015**, *16*, 2121–2127. [[CrossRef](#)]
9. Lee, S.-J.; Katayama, S.; Kim, J.-D. Microstructural behavior on weld fusion zone of Al-Ti and Ti-Al dissimilar lap welding using single-mode fiber laser. *J. Korean Soc. Mar. Eng.* **2014**, *38*, 133–139. [[CrossRef](#)]
10. Zhang, Y.; Gao, X.; You, D.; Jiang, X.; Ge, W. Investigation of Laser Butt Welding of AISI 304L and Q235 Steels Based on Numerical and Experimental Analyses. *Metals* **2022**, *12*, 803. [[CrossRef](#)]
11. Zhou, H.; Fu, F.; Dai, Z.; Qiao, Y.; Chen, J.; Liu, W. Effect of Laser Power on Microstructure and Micro-Galvanic Corrosion Behavior of a 6061-T6 Aluminum Alloy Welding Joints. *Metals* **2021**, *11*, 3. [[CrossRef](#)]
12. Lee, S.J.; Sharma, A.; Jung, D.H.; Jung, J.P. Influence of Arc Brazing Parameters on Microstructure and Joint Properties of Electro-Galvanized Steel. *Metals* **2019**, *9*, 1006. [[CrossRef](#)]
13. Lee, S.-J.; Katayama, S.; Kawahito, Y.; Kim, J.-D.; Suh, J. Weld Plume Behavior during Laser Lap Welding of Al and Ti Dissimilar sheets. In Proceedings of the 35th International Congress on Applications of Lasers & Electro-Optics (ICALEO@2016), San Diego, CA, USA, 16–20 October 2016; p. 407.
14. Wang, L.; Zhang, G.; Xu, J.; Li, Y.; Chen, Q.; Rong, Y.; Huang, Y. Effect of Welding Parameters on the Geometry, Microstructure, and Corrosion Resistance of Laser Welded 16 mm EH40 Joints. *Metall. Mat. Trans. B* **2021**, *52*, 3930–3937. [[CrossRef](#)]
15. Kim, J.; Kim, Y.; Kim, J.; Kim, Y.; Kim, D.; Kang, S.; Pyo, C. A Study on Lap Joint Welding of Thin Plate ASTM F1684 Using Fiber Laser Welding. *Processes* **2021**, *9*, 428. [[CrossRef](#)]
16. Oh, R.; Kim, D.Y.; Ceglarek, D. The Effects of Laser Welding Direction on Joint Quality for Non-Uniform Part-to-Part Gaps. *Metals* **2016**, *6*, 184. [[CrossRef](#)]
17. Arya, H.; Singh, K.; Singh, S. Cooling Rate Effect on Microhardness for SAW Welded Mild Steel Plate. *Int. J. Theo. Appl. Res. Mech. Eng.* **2013**, *2*, 71–77.
18. Zhao, H.; Qi, H. Numerical Simulation of Transport Phenomena for Laser Full Penetration Welding. *J. Weld. Join.* **2017**, *35*, 13–22. [[CrossRef](#)]
19. Ferro, P.; Bonollo, F.; Tiziani, A. Laser welding of copper–nickel alloys: A numerical and experimental analysis. *Sci. Tech. Weld. Join.* **2005**, *10*, 300–310. [[CrossRef](#)]
20. Katayama, S.; Kawahito, Y.; Mizutani, M. Elucidation of laser welding phenomena and factors affecting weld penetration and welding defects. *Phys. Procedia* **2010**, *5*, 9–17. [[CrossRef](#)]
21. Wang, C.; Wang, C.; Gao, X.; Tian, M.; Zhang, Y. Research on Microstructure Characteristics of Welded Joint by Magneto-Optical Imaging Method. *Metals* **2022**, *12*, 258. [[CrossRef](#)]
22. Sadeghian, A.; Iqbal, N. Blue laser welding of low thickness Ni-coated copper and mild steel for electric vehicle (EV) battery manufacturing. *Opt. Laser Tech.* **2022**, *155*, 108415. [[CrossRef](#)]
23. Mathivanan, K.; Plapper, P. Laser welding of dissimilar copper and aluminum sheets by shaping the laser pulses. *Procedia Manuf.* **2019**, *36*, 154–162. [[CrossRef](#)]
24. Dimatteo, V.; Ascari, A.; Fortunato, A. Dissimilar laser welding of copper and aluminum alloys in multilayer configuration for battery applications. *J. Laser Appl.* **2021**, *33*, 042028. [[CrossRef](#)]
25. Lei, Z.; Zhang, X.; Liu, J.; Li, P. Interfacial microstructure and reaction mechanism with various weld fillers on laser welding-brazing of Al/Cu lap joint. *J. Manuf. Process.* **2021**, *67*, 226–240. [[CrossRef](#)]
26. Mohan, D.G.; Tomków, J.; Karganroudi, S.S. Laser Welding of UNS S33207 Hyper-Duplex Stainless Steel to 6061 Aluminum Alloy Using High Entropy Alloy as a Filler Material. *Appl. Sci.* **2022**, *12*, 2849. [[CrossRef](#)]
27. Fabbro, R. Depth Dependence and Keyhole Stability at Threshold, for Different Laser Welding Regimes. *Appl. Sci.* **2020**, *10*, 1487. [[CrossRef](#)]
28. Fabbro, R. Keyhole modeling during laser welding. *J. Appl. Phys.* **2000**, *87*, 4075–4083. [[CrossRef](#)]
29. Fabbro, R. Melt pool and keyhole behavior analysis for deep penetration laser welding. *J. Phys. D Appl. Phys.* **2010**, *43*, 445501. [[CrossRef](#)]